Fate and transport of enveloped viruses in indoor built spaces – through understanding vaccinia virus and surface interactions

Dahae Seong, Monchupa Kingsak, Yuan Lin, Qian Wang, Shamia Hoque

Key Words:
adhesion kinetics; aerosols; built environment; resuspension; surface properties; ventilation

From the Contents

ABSTRACT

The current coronavirus disease 2019 (COVID-19) pandemic has reinforced the necessity of understanding and establishing baseline information on the fate and transport mechanisms of viruses under indoor environmental conditions. Mechanisms governing virus interactions in built spaces have thus far been established based on our knowledge on the interaction of inorganic particles in indoor spaces and do not include characteristics specific to viruses. Studies have explored the biological and kinetic processes of microbes' attachments on surfaces in other fields but not in the built environment. There is also extensive literature on the influence of indoor architecture on air flow, temperature profiles, and forces influencing aerosol transport. Bridging the gap between these fields will lead to the generation of novel frameworks, methodologies and know-how that can identify undiscovered pathways taken by viruses and other microbes in the built environment. Our study summarizes the assessment of the influence of surface properties on the adhesion kinetics of vaccinia virus on gold, silica, glass, and stainless-steel surfaces. We found that on gold the virus layer was more viscoelastic compared to stainless-steel. There was negligible removal of the layer from the stainless-steel surface compared to the others. The results further highlight the importance of converging different fields of research to assess the fate and transport of microbes in indoor built spaces.

***Corresponding author:**
Shamia Hoque,
hoques@cec.sc.edu.

http://doi.org/10.3877/cma.j.issn.2096-112X.2021.01.007

How to cite this article:
Seong, D.; Kingsak, M.; Lin, Y.; Wang, Q.; Hoque, S, Fate and transport of enveloped viruses in indoor built spaces – through understanding vaccinia virus and surface interactions. *Biomater Transl.* **2021**, *2*(1), 50-60.

Introduction

The significance of the built environment and the materials that construct it has become critical during the ongoing pandemic. How long does the severe acute respiratory syndrome coronavirus 2 (SARS-CoV-2) survive in the air and on surfaces? Since the pandemic hit this has been a perpetual question with the answer still being investigated. It is well known that contaminated surfaces are significant vectors in the transmission of infection both in hospitals and in the community.[1, 2] Recent investigations[3] into determining stability of the virus on different surfaces and in the aerosolized form revealed that the SARS-CoV-2 virus can survive for 3 hours in the aerosolized form and 72 hours on plastic and stainless steel[4] with survivability varying based on indoor and outdoor conditions.[5, 6] The transmission forms for both SARS-CoV-1 and SARS-CoV-2 are similar.[3, 7] Studies on transmission routes for influenza virus have documented the dominant influence of airborne transmission via suspended and settled droplets[8-10] resulting in guidelines of social distancing (~6 feet, about 1.83 m) to prevent person to person transmission.[11]

The studies all focus on obtaining data on either the influence of air circulation such as sampling in an aerosolized environment or via inoculating different types of surfaces. The investigations do not account for the fact that the two events are not isolated. Aerosolized virus laden droplets must be transported to the boundaries near the surfaces, deposit from the boundary layer on to the surface and subsequently adhere. Recent

events have also shown the high probability of aerosolized transmission.[12-14] The question that needs to be answered to successfully limit transmission is, "What conditions control the transport, deposition, adhesion, and persistence of airborne SARS-CoV-2 in air and on surfaces?" The interface of the boundary layer and the surface influences the transport and deposition of particles including virus laden droplets. **Figure 1** illustrates the concept. The fluid mechanical boundary layer is the flow region (air) very near the surface where viscous forces dominate and transitions to a region of high velocity of air.[15] Air flow in indoor spaces is often treated as well mixed but, investigations have shown the significant influence of near surface air motion on particle deposition[16] and resuspension.[17]

There is however a lack of information on the relationship between the magnitude of shear forces and boundary flow velocity characteristics on the transport mechanism of viruses particularly near surfaces. Released virus droplets or aerosolized viruses will over time reach the boundary layers near the surface where they will subsequently 'attach' to the surface and adhere to it. Investigations in aqueous suspensions have shown the wide ranging and variable influence of wall shear rates on the deposition, adhesion and detachment of particles and microbes.[18-20] The attachment process is influenced by the surface characteristics which include surface roughness (RH), porosity or morphology, or microbial characteristics which are mobility, flexibility, or hydrophilicity.[21, 22]

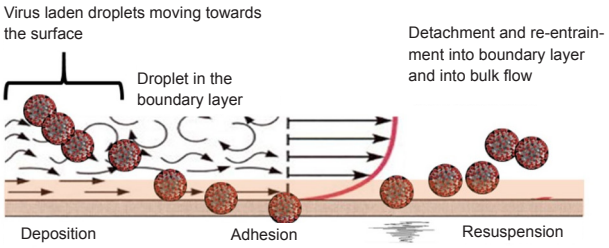

Figure 1. Schematic illustration of the fate and transport of virus particles at the intersection of bulk and boundary layer flow.

To gain insight on these processes and their influence on the fate and transport of microbes in the indoor space, the authors assessed the adhesion behavior of a model enveloped virus, vaccinia virus (VACV), on various types of surface seen in the built environment under flow conditions. The investigation is a prelude to further studies on how the complex interaction of the multiple variables of an indoor space can influence the fate and transport of microbes in the bulk flow and boundary layer. This article also summarizes the current knowledge on particle deposition, attachment and re-entrainment in indoor spaces and the influence of properties of materials on the particle transport behavior. The paper concludes by discussing the results of the authors' work in context of past investigations and future directions.

Methods

VACV culturing and purification

Vero cells (Centers for Disease Control and Prevention, Atlanta, GA, USA) were cultured in Dulbecco's modified Eagle's medium (Corning, Manassas, VA, USA) supplemented with 10% fetal bovine serum (Atlanta Biologicals, Flowery Branch, GA, USA), 2 mM L-glutamine, 1 mM sodium pyruvate, and 100 U/mL penicillin-streptomycin (HyClone, Marlborough, MA, USA). Cell cultures were maintained at 37°C in a CO_2 incubator with 5% CO_2 and 95% air. VACV was propagated in Vero cells with the presence of 2% fetal bovine serum Dulbecco's modified Eagle's medium. The infected cells were incubated at 37°C for 2 to 4 days until the microscopic cytopathic effect was complete.

The virus purification method was modified from Hruby et al.[23] In brief, the infected cells were harvested and subjected to homogenization. Cell debris was removed by centrifugation at 12,296 × *g* for 15 minutes at 4°C (Sorvall® RC5C plus, Newtown, CT, USA). The virus pellets were precipitated by centrifugation at 81,799 × *g* for 3 hours at 4°C (Beckman L8-70M, Palo Alto, CA, USA) and resuspended in 1 mM Tris buffer (pH 8) overnight. Purified virus was obtained through a side-band-pull from a gradient of sucrose centrifuged at 22,504 × *g* for 40 minutes at 4°C. Vero cells were plated in 6-well plates at a density of 6×10^5 cells per well one day prior experiment. Ten-fold serial dilutions of purified virus were made in phosphate buffered saline. The virus samples of each dilution were placed onto the prepared 6-well plate cultured with Vero cells, then incubated at room temperature in a laminar flow hood for 30 minutes. After infection, unbound virus was removed and replaced with 1% agarose (VWR Life Science, Radnor, PA, USA) in 2% fetal bovine serum Dulbecco's modified Eagle's medium. The plates were incubated at 37°C and 5% CO_2 for 2 to 4 days until able to visualize plaques. The virus titer was calculated using an average number of plaques, dilution factor, and the inoculum volume as described elsewhere.[24]

Quartz crystal microbalance with dissipation analysis

The quartz crystal microbalance with dissipation (QCM-D) approach was applied to investigate virus adhesion and detachment on four types of sensor surfaces.[25, 26] QCM-D

Department of Civil and Environmental Engineering, University of South Carolina, Columbia, SC, USA

technique was performed using Q-sense E4 (Biolin Scientific, Gothenburg, Sweden). Polished AT-cut 5-MHz quartz crystals coated with four materials were selected: gold (QSX 301) with RH < 1 nm, SiO_2 (QSX 303) with RH < 1 nm, sodalime-glass (QSX 337) with RH < 20 nm, and stainless-steel (QSX 304) with RH < 1 nm. Temperature in the modules was controlled at 23°C. Three flow rates were assessed: 8.33×10^{-6} m^3/s (50 µL/min), 1.67×10^{-6} m^3/s (100 µL/min), and 3.33×10^{-6} m^3/s (200 µL/min). Before the experiment, all sensors were pre-cleaned with ultraviolet/ozone light for 10 minutes to remove organic contaminants on the surface. MilliQ water was first injected into the modules to provide a baseline measurement. Then, virus suspension suspended in 1 mM Tris buffer was injected at a selected flow rate. Experiments were initiated at four initial concentrations, 6.45×10^4, 2.00×10^5, 2.25×10^5 and 2.68×10^5 plaque-forming unit/mL. Virus attachment resulted in the decrease of frequency and increase of dissipation. Once both frequency and dissipation attained a constant value, the modules were rinsed with the baseline solution. Changes of frequency (Δf) and dissipation (ΔD) on the sensor crystal were recorded using QSoft401 and the data were analyzed using QSense Dfind software (Biolin Scientific). Before the start of any experiment and in between each experiment, QCM-D modules and sensors were thoroughly cleaned using a 2% sodium dodecyl sulfate solution (Fisher Scientific, Waltham, MA, USA) and ultraviolet/ozone treatment and dried with N_2 gas.

The QCMD detects mass and dissipation change through the excitation of the sensor crystal which oscillates at a specific frequency due to the application of a certain voltage across the electrodes because of piezoelectric properties.[27, 28] Mass change (Δm) on the sensor crystal causes frequency change (Δf) and is defined by Sauerbrey relation as shown in equation (1) where c is 17.7 ng/Hz/cm^2 for a 5-MHz crystal, and n is the overtone.

$$\Delta m = -\frac{\Delta f \times c}{n} \quad (1)$$

Dissipation (D) is caused by the adsorption of the viscoelastic film and is described as the ratio of dissipated and stored energy.[29, 30] Energy lost during crystal oscillation is calculated using the measured dissipation based on equation (2) where, where E_{diss} is the energy dissipated during one oscillatory cycle and E_{strd} is the energy stored in the oscillation system.[31, 32]

$$D = \frac{E_{diss}}{2\pi E_{strd}} \quad (2)$$

Characterization of virus coated surfaces

Atomic force microscopy

Glass slides were cleaned by Piranha solution (30% hydrogen peroxide and concentrated sulfuric acid with 3:7 ratio from Fisher) at 75°C for 2 hours following by washed and sonicated in MilliQ water. The cleaned glass slides were then immerged in 1 mg/mL poly(diallyl dimethylammonium chloride) (PDDA) solution overnight, rinsed with MilliQ water (Millipore, Burlington, MA, USA) and dried with N_2 gas. PDDA (molecular weight 100,000 to 200,000) was purchased from Sigma-Aldrich (St. Louis, MO, USA). The PDDA-glass substrate was then immerged in VACV solution at the concentration of 1×10^4 plaque-forming unit/mL for 1 hour, gently rinsed with water and dried with N_2 gas. Atomic force microscopy images of VACV on glass slides and RH were obtained by SPA 300 instrument (Veeco, Santa Barbara, CA, USA) in ambient conditions under tapping mode at a scan rate of 1 Hz and scan size of 10×10 µm^2.

Fluorescence microscopy

A recombinant VACV expressing green fluorescence protein was placed onto a glass slide and evaporated to dryness in a laminar flow hood. The excessive green fluorescence protein-tagged viruses were gently washed out by phosphate buffered saline solution. The fluorescence images were acquired using a fluorescent microscope (Olympus IX81, Shinjuku-ku, Tokyo, Japan) with disk scanning unit confocal mode.

Zeta potential measurement

The purified virions were incubated for 5 minutes and overnight in 1 mM Tris buffer pH 8 and pH 4.5. The virus samples were then transferred to a DTS1070 disposable capillary cell (Malvern, Malvern, Worcestershire, UK) for zeta potential measurements. The measurements were performed at 25°C with a Zetasizer Nano-ZS (Malvern).

Transmission electron microscopy imaging

The virus was dropped onto a carbon coated copper grid for 30 minutes, and the excess virus solution was blotted off. The grid was washed with several drops of MilliQ water and dried by slow evaporation in air at room temperature. After the adsorption, 2% uranyl acetate was applied to the grid for negative staining. The morphology of the purified VACV was characterized by Transmission electron microscopy (Hitachi HT7800, Chiyoda-ku, Tokyo, Japan).

Results

VACV characteristics

VACV, a member of the poxvirus family, is an enveloped virus.[33] It consists of a large double-stranded DNA genome approximately 190 kb in length, a protein layer known as the palisade, and the envelope composed of surface tubules, enveloped proteins, and lipid membranes, as illustrated in **Figure 2A**.[34-37] VACV has an oval to brick-shaped architecture with the dimensions of 270 nm in diameter and 350 nm in length.[35, 36] The purified VACV using in this study expresses green fluorescence protein and can be observed under a fluorescent microscope as shown in **Figure 2B**. Surface charge of the virus is one of the important factors that play an essential role in numerous sorption processes, for example adsorption and adhesion, which are governed by electrostatic interactions.[38] To investigate the physical and charge characteristics of the purified virions, atomic force microscopy and dynamic light scattering were performed. In **Figure 2C**, VACV shows a negative surface charge with a zeta potential of approximately –30 mV in pH 8 Tris buffer solution and –20 mV in pH 4.5 Tris buffer solution, incubated in the buffers for 5 minutes and overnight, using Zetaseizer. In addition, atomic force microscopy revealed that a good deposition of negatively

charged virions on a positively charged PDDA-glass substrate was found (**Figure 2D**). The average size of VACV is ~200–350 nm in different directions as observed under transmission electron microscope (**Figure 2E**), which is consistent with literature survey.[39-41]

Virus adhesion kinetics via QCM-D

Table 1 shows the details of the frequency and dissipation shifts for both adhesion and detachment, and **Figure 3A–D** display the frequency (Δf), and dissipation (ΔD) shifts of the third overtone. Four types of sensors were applied to investigate the relation between the types of sensor material and virus adhesion, gold, silica, glass, and stainless-steel (SS).

MilliQ water was first entered for a baseline. A stable baseline was observed prior to VACV injection regardless of the type of sensor material. The black arrows indicated the injection of VACV (2.0×10^5 plaque-forming unit/mL). At 4 minutes, sensors were exposed to the virus suspension, thus, rapid decrease in frequency was observed due to sensor – virus bindings. Rapid increase in dissipation was observed corresponding to the virus adhesion to the sensor surface. The frequency and energy dissipation were monitored in real time while the virus adhesion resulted in the built up of multilayers on the sensor crystals. When no more significant changes in frequency and dissipation were observed, MilliQ water (blue arrows in **Figure 3A–D**) flow was started to rinse the sensor surface and to measure the virus detachment, concurrently. Gold sensor resulted in the smallest change of frequency, Δf = –5.77 Hz while silica had the maximum frequency shifts of –31.70 Hz. Glass had a frequency shift of –29.81 Hz while SS exhibited a frequency shift between silica and glass, –22.16 Hz. ΔD for all sensors ranged from 1.85×10^{-6} to 2.52×10^{-6}. Increase in frequency and decrease in dissipation were observed due to virus detachment and is an indicator of virus – surface adhesion characteristics i.e., whether the film layers formed is soft or rigid or became rigid due to multi-layer formation. Even though increase in frequency and decrease in dissipation were measured after rinsing, the values did not return to baseline levels. This indicates that the cleaning step washed away soft layers, but remaining layers on the sensor crystals had become rigid and could not be 'cleaned' thoroughly to negligible values. **Figure 3E** shows the calculated mass of virus layers after adhesion and then after rinsing i.e., extent of detachment applying the Sauerbrey relation. For SiO_2, 13% of mass was removed after rinsing (189.1 ng/cm^2 of adsorbed virus layer and 164.6 ng/cm^2 of remained virus layer), followed by glass, 9% (177.8 and 162.4 ng/cm^2), gold, 7% (34.4 and 32.0 ng/cm^2). The lowest removal occurred for stainless-steel after rinsing (132.2 and 126.7 ng/cm^2).

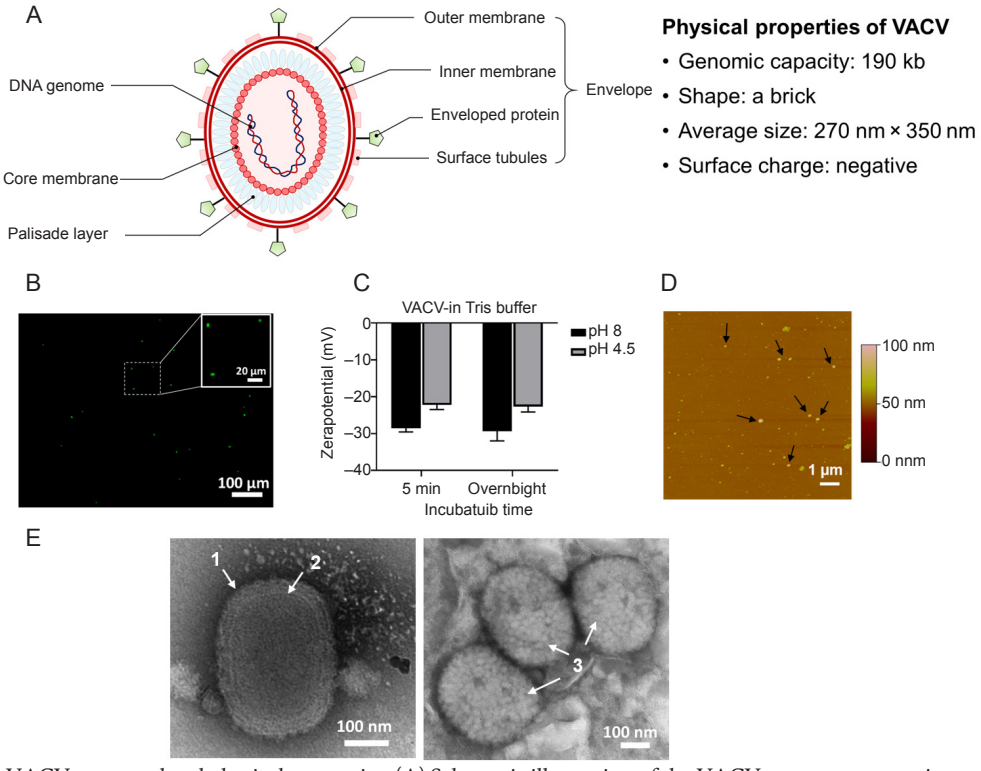

Figure 2. VACV structural and physical properties. (A) Schematic illustration of the VACV structure, genomic capacity, shape, average size, and surface charge. (B) Fluorescence imaging of green fluorescence protein-tagged VACV (green). (C) Zeta potentials of VACV over the pH 8 and pH 4.5 in 1 mM Tris buffer. Data are expressed as mean ± SD. (D) Atomic force microscopy image of VACV deposited on PDDA-glass substrate. The black arrows point to VACV particles. (E) Representative transmission electron microscopic images of VACV. The white arrows point to (1) outer membrane, (2) core membrane, and (3) surface tubules. Scale bars: 100 μm in B, 20 μm in enlarged part in B, 1 μm in D and 100 nm in E. PDDA: poly(diallyl dimethylammonium chloride); VACV: vaccinia virus. The duplicate samples were measured and two experiments were repeated to acquire the data.

Table 1. Frequency (Δf) and dissipation (ΔD) shift due to VACV adhesion and mass (Δm) of adhered VACV on the sensor surface calculated by Sauerbrey relation

Sensor	VACV adhesion		VACV detachment	
	Δf (Hz)	ΔD ($\times 10^{-6}$)	Δf (Hz)	ΔD ($\times 10^{-6}$)
Gold	–5.77	1.90	–5.37	1.39
SiO_2	–31.70	1.85	–27.60	0.98
Glass	–29.81	2.52	–27.22	1.72
Stainless-steel	–22.16	2.40	–21.23	2.11

Note: VACV: vaccinia virus. This is representative of an experiment started at 2.00×10^5 plaque-forming unit/mL.

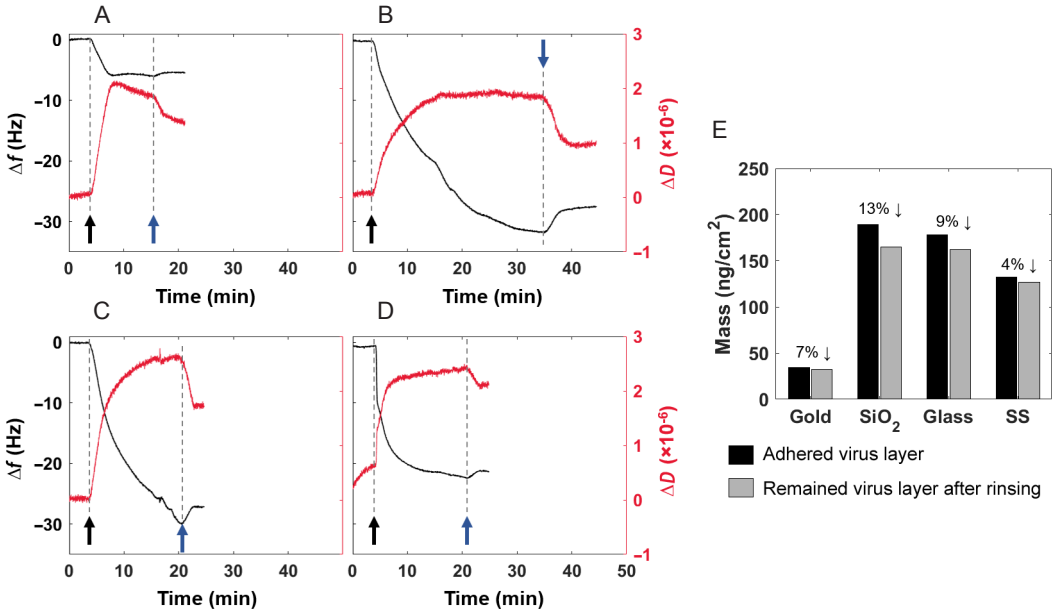

Figure 3. Quartz crystal microbalance with dissipation analysis of the frequency (Δf, black line) and dissipation (ΔD, red line) ($\times 10^{-6}$) shifts of VACV on gold (A), SiO_2 (B), glass (C), and stainless-steel (D). Black arrow: VACV injection; blue arrow: rinsing with MilliQ. (E) Mass of adhered and remained virus layer on the sensor surfaces calculated by Sauerbrey relation. SS: stainless-steel; VACV: vaccinia virus. This is representative of an experiment started at 2.00×10^5 plaque-forming unit/mL.

Figure 4 displays the *f*–*D* plots to assess the structural conformation of the adhered VACV layers. The slope (K, $\Delta D/\Delta f$) represents the adsorption kinetic process on the sensor crystal. Higher K indicates the structural conformation of the layer on the sensor surface is soft and flexible whereas lower K represents that the layer is thin and rigid. Initially a soft layer (K_1) is formed while as it adheres to the sensor surface and then the layer becomes firm (K_2). After the rinsing step, part of the adhered layer has been removed from the sensor (increase in frequency) and the remaining layer is more rigid (K_3).

Figure 4A shows the adsorption process for VACV-gold. In comparison to **Figure 4B–D** which represents the adhesion process of VACV for silica, glass, and SS respectively, K_1 and K_2 is the steepest for gold sensor indicating the layer attached is more viscoelastic compared to the others. The sensor also has the lowest K_3 value which indicates that the layer remaining is thin, and rigid as opposed to its counterparts. **Figure 4B** and **C** show similar characteristics of the layer formed initially at the beginning of adherence of VACV to silica and glass. K_2 and K_3 values for silica are less than glass. VACV-SS interaction based on K_1, K_2 and K_3 is very similar in magnitude to glass. SS surface is positively charged[42] and the extent of detachment of negatively charged VACV is significantly less compared to the other sensors.

Discussion

The results focus on one aspect of the multi-faceted problem – influence of surface type on attachment and detachment of VACV. The significance of understanding how surface properties control the adhesion kinetics is highlighted. During the initial adhesion process the viscoelastic nature of the virus layer was dependent on the surface type. After the first phase of attachment, there is a plateau indicating saturation has been reached and the layer is becoming rigid. Rinse cycle is started immediately, and the extent washed off differs based on the properties of the layer formed and for these surface types, surface charge. Gold behaves very differently from the other surfaces, in that while mass attached is lower than SS, it remains attached. Glass and silica appear to be the 'cleanest' surfaces since adhered viruses were easily cleaned compared to other surfaces. The effect of 'flow' on the behavior of VACV-surface interactions remains to be investigated and correlated. In the sections below the factors that can influence fate and transport of aerosols including microbes are discussed.

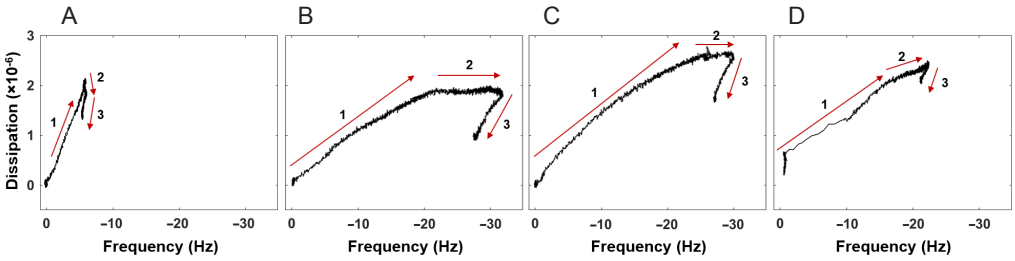

Figure 4. Frequency-dissipation plots for VACV for gold (A), SiO_2 (B), glass (C), and stainless-steel (D). '1', '2', and '3' show the steps of the adhesion process, '1' adhesion, '2' reaching saturation and '3' detachment due to the wash cycle. The numbers correspond to the slope represented by K_1, K_2 and K_3. VACV: vaccinia virus. This is representative of an experiment started at 2.00×10^5 plaque-forming unit/mL.

Phenomena influencing deposition

Extensive investigation in the factors influencing deposition of inorganic particles has been done because of the significant role it plays on human health and exposure. The deposition phenomena are influenced by multiple factors which include particle characteristics, air flow, interior design, and surface coverings.[43-46] The interacting effect of ventilation, location of furniture and air changes have shown that while higher air changes removed particles faster, localized exposure and deposition is influenced by a combination of multiple factors.[47] Experimental and modeling studies determined a lumped parameter: deposition velocity or loss rate coefficient for a range of particle sizes to distinguish the effects of the multi-dimensional design space which describe the indoor environment.[48,49] Deposition velocities and loss rate coefficients provide a bulk perspective of the transport and removal of particles from the air.[50] The rate at which deposition occurred is represented by deposition velocity, v_d as shown in $v_d = \frac{M}{tCA_s}$ where M is the mass of particle on a sample surface, t is time of exposure, C is time-weighted average mass concentration of particles in air and A_s is the surface sample area.

Studies in small scale chambers and real houses have shown that particle removal by deposition is significantly correlated to diameter, surface to air temperature difference, surface orientation, spatial location, and RH.[43,46,49] Deposition constants have been shown to be related to building wall textures, orientation and particle size.[51] Among surface properties, the influence of RH has been assessed. Lai and Nazaroff[52] observed that particle deposition increased for most particle sizes onto smooth and rough vertical surfaces, with roughness simulated using smooth glass plates and sandpaper. While deposition clearly increased with near wall airflow velocity the influence of RH became less evident[48] probably due to the dominance of the fluid momentum boundary layer.

Deposition velocities in relation to microbe carrying particles or for microbes have not been investigated extensively. Typically, the studies incorporate properties or stay within the range of parameters accepted for inorganic particles. For example, a computational fluid dynamics model based on Eulerian-Lagrangian framework simulated the deposition of *Staphylococcus* and *Micrococcus*, the conclusions identified that mixing and ventilation conditions influenced deposition of the bacterial species.[53] The spherical species have a diameter ~1 μm and were selected because of the proximity of the physical characteristics for the application of stokes' law and lack of information for microbes. Studies cannot account for the characteristics of the different types of microbes, bacteria, viruses, and fungi which can influence transport and deposition. Whyte and Eaton[54] calculated deposition velocities as a function of concentration of airborne particles carrying microbes by collecting samples from clean rooms and operation theatres. They reported higher deposition rates for lower concentrations. Seong and Hoque[55] assessed the influence of sampling region and sampling location on bacterial species detected.

Adhesion forces governing surface interaction

The forces encountered in adhesion of solid particles on solid surfaces either in air (at different humidity levels) or in water or other media are molecular interactions defined by Van der Waals' forces, electrostatic interaction, liquid bridges, double layer interaction and polar and/or metallic bonds.[56-59] Dust and activated carbon appear to preferentially adhere to insulated surfaces such as polyvinyl chloride or glass compared to aluminum and copper.[60] Physics-based model such as the Hamaker model depending exclusively on Van der Waals forces was not successful in interpreting the adhesion mechanism and results indicated the significance of considering polar contributions.[60,61] Other investigations have looked into particle shape and size pointing out the limitation that most studies tend to focus on spherical particles.[62,63]

Deryaguin–Muller–Toporov, Johnson–Kendall–Roberts and Maugis–Pollock models[64-66] have been applied to describe molecular attraction forces and the influence of contact areas between particles and surfaces. RH and contact angle have a high impact on the magnitude of the Van der Waals forces. Higher humidity levels, beyond 50% tend to enhance adhesion;[56,61] however, the hydrophilic/hydrophobic nature of particles and surfaces impacts the degree of influence.[67] For example, adhesion force of glass on glass or glass on silica surfaces for diameters ~20 to 60 μm treated to be hydrophobic remained constant for all humidity levels while for hydrophilic conditions, at 50–60% humidity adhesion force increases or resuspension decreased.[68] The anomaly observed for hydrophobic surfaces and the increasing deviation from classical theoretical predictions for larger size particles have been attributed to the water film formed between particles

and surfaces and/or the electrostatic forces. Adhesion force magnitudes decreasing with particle size.[56] Particles of size in the range > 1 μm to ~5 μm adherence to surfaces is determined by the nature of the contact and are harder to resuspend but larger size particles are easier to resuspend and the adhesion mechanism is influenced by contact points, and geometry.[57, 69]

This literature survey on adhesion of microbiological particles to surfaces target bacteria and viruses. Studies focusing on bacteria are dominated by areas such as biocorrosion,[70] biomaterial implants,[71, 72] environmental microbiology,[73] food industry,[74] and microbial fuel cells.[75] The adhesion mechanism is modeled typically using the Derjaguin, Landau, Verwey, Overbeek (DLVO) approach, or the thermodynamic approach or the extended DLVO model.[76-79] The DLVO theory is based on the non-specific interaction energies between the van der Waals forces and the electrostatic double layer forces which can be attractive or repulsive contingent on the bacteria-surface combination. Thermodynamic theory on the other hand is based on the concept of surface free energies which would account for the various types of interactions including van der Waals, electrostatic and dipole moments. Since the DLVO theory assumed inert chemical surfaces, a modification was added to the theory by adding a short-range Lewis acid-base term which will account for the hydrophobicity/hydrophilicity in an extended DLVO theory.[80]

The extended DLVO theory has been applied to shed light on the mechanisms governing the adhesion of viruses to certain surfaces. For example, a study by Chrysikopoulos and Syngouna[81] looked at the interaction of bacteriophages, MS2 and ΦX174 with clay colloids. The virus attachment was described by the Freundlich isotherm and the Lewis acid-base term in the extended DLVO model was critical in explaining the hydrophobic interaction mediated attachment. The extended DLVO approach was utilized to model the attachment of human adenoviruses and two bacteriophages, P22 and MS2[82] to lip balms. The study showed that drying of the lip balms resulted in the drop of surface free energy which made the surfaces highly hydrophobic. The extended DLVO model results predicted that attachment was favored due to short range strong hydrophobic interaction. Hydrophobic and electrostatic interactions were also shown to govern the attachment of MS2 bacteriophage to surfaces treated with polyelectrolyte multilayers.[83]

Recent investigations have tried to unravel the implications of virus adhesion kinetics with regard to health effects, infection transmission and SARS-CoV-2[4,84-86] by utilizing representative surrogates such as a lentivirus[85] or through conducting a theoretical analysis utilizing existing data to assess the influence of different surfaces and environmental conditions including temperature, humidity, and pH.[6, 84, 87] Experimental methods for determining the adhesion force and kinetic mechanisms include using the centrifuge approach[88, 89] or the QCM-D[82, 83, 90] and AFM.[91, 92] Liu et al.[93] used floor dust as surrogates for fungal spore and high-speed imaging to capture the effect of velocity on resuspension. For microbes and surfaces of the built environment, investigation has focused on antimicrobial properties of metal alloys such as copper – zinc, copper – silver on surfaces and their application.[94-97] The studies highlight the significant differences that exist between the adhesion mechanisms for inorganic particles versus microbes.[98]

The mechanism of resuspension

Measurements of resuspension have been expressed as resuspension factors or resuspension rates.[99] Resuspension factor is the ratio of air borne contaminant concentration per unit air volume to the contaminant surface concentration per unit area on the ground and resuspension rate is defined as the fraction of a surface species removed in unit time.[99]

Experimental results showed that smaller particles required larger flow velocity to achieve the same amount of detachment as the larger particles. The detachment fraction was also dependent on the surface adhesion energy of the particles ranging between ~32 μm and ~76 μm with higher velocities required for higher adhesion energy.[100] Punjrath and Heldman[101] studied particle entrainment in a wind tunnel and theorized that two mechanisms: a) initiation of particle movement when shear stresses on the particles exceed friction forces acting on the particles and b) transfer of momentum from other moving particles dominated resuspension.

Modeling studies comprised of two approaches – statistical and/or force balance. Theoretical models have simulated the mechanisms at a micro scale,[17, 102-104] whereas computational fluid dynamics models have focused on capturing the movement of a specific activity such as foot tapping[62] and analytical models[105] have applied multiple fundamental concepts such as dimensional analysis to model the effects. The Eulerian method, in which particles are treated as a continuum, has been traditionally applied to the cases of heavy particle deposits while Lagrangian methods have been applied to individually track relatively light particles in monolayer or few multi-layer systems.[106, 107] In Lagrangian-based models, particle transport is generally modeled through the addition of gravitational, drag, added mass, Saffman's lift, bed impact forces and Bassett forces.[108] Among these forces, Bassett forces (force due to acceleration of the particle) have been considered negligible and bed impact forces are more dominant than lift forces. Braaten et al.[102] assumed that fluid forces are applied at the surface in discrete 'bursts' following a probability distribution. Saffman's lift force[109] has been used in the literature to describe the particle motion when studying particle deposition mainly. Mollinger and Nieuwstadt[110] and Leighton and Acrivos[111] also developed expressions for the lift force for particles touching the wall. Shi and Bayless[112] developed a computational fluid dynamics model of a gas-particle flow in cyclones. The authors incorporated a balance of adhesion and lift-off forces to account for particle detachment from the surfaces.

Due to the inherent random nature of particle behavior, statistical approaches for predicting resuspension such as Monte Carlo simulations[113] and Lagrangian stochastic models have been proposed.[114] The stochastic models showed that resuspension can be captured numerically but appropriate attention needs to be given to fluctuations created due to

turbulent flow or bursts created due to surface impacts.[17, 103] Loosmore[99] developed empirical models to calculate resuspension rate, using five parameters: friction velocity, time since the wind flow begin, particle diameter, particle density, and roughness height and identified friction velocity and time of exposure as the most important factors. In an indoor space particle resuspension magnitude could vary by two to three orders of magnitude. Resuspension rates between 3×10^{-7} and 6×10^{-6} min^{-1} were found for super micron particles of density 1000 kg/m^3. Substantial resuspension of particles of diameter 2.5 μm and 5 μm occurred with source strengths ranging from 0.03 mg/min to 0.5 mg/min, a range estimated for human activities.[43, 44, 115]

Few studies have explored the effects of resuspension of microbes. Krauter and Biermann[116] examined the reaerosolization of dry spores (0.6–1.1 μm) in a ventilation duct. Resuspension rates of fungal spores on both steep and plastic duct materials were between 6×10^{-2} and 6×10^{-4} min^{-1}, which decreased to 10 times less than the initial rates within 30 minutes. In depth analysis of the influence of friction, RH, exposure time and forces which have been assessed to an extent for particles have not been quantified regarding bacteria, viruses, or fungi.

Conclusions

The current pandemic has reinforced the necessity of establishing baseline information on how viruses under indoor environmental conditions optimize survivability and transmission. Based on the discussions above, investigations into understanding this phenomenon can be separated into three main categories. One category investigates the effects of indoor environmental factors and surface properties on boundary flow characteristics. The second group of studies assesses the influence of the same variables on various phenomena such as drag force, electrostatic force or thermophoretic force which effects aerosol fate and transport. The last category is the effect of physical and biological properties on the deposition, attachment, and persistence of microbes on surfaces. Typically, the three categories discussed are investigated independent of each other with some overlap occurring in categories 1 and 2. But, an indoor environment with a range of bacteria, viruses and fungal species, and an evolving microbial world encompasses all three categories as shown in **Figure 5**. To successfully understand, assess, and predict how the indoor environment perpetuates transmission, we must bridge the gaps between these fields.

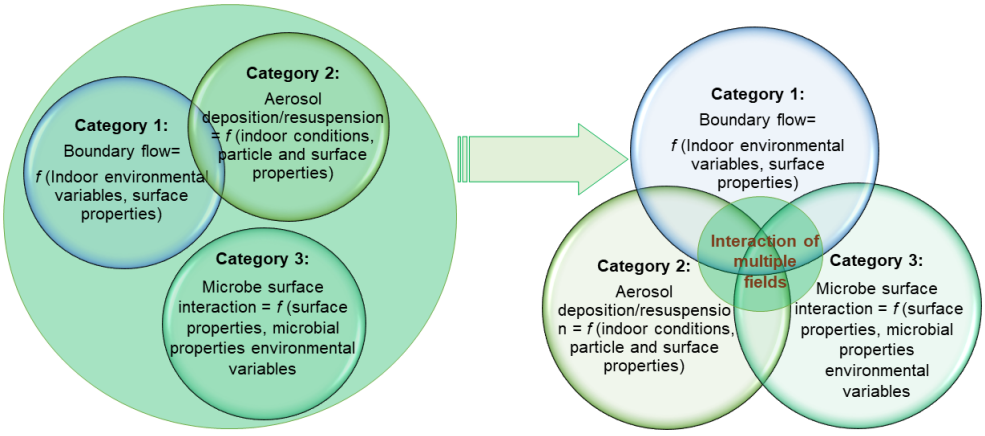

Figure 5. A schematic representation of the current state and future research directions. f: function.

Author contributions

Study concepts: SH and QW; study design: SH, DS, MK, YL and QW; previous studies analysis and manuscript review: SH, DS, MK and QW; experiment implementation and data analysis: DS, MK and YL; data acquisition: DS and MK; manuscript preparation: SH, DS and MK; manuscript editing: SH, DS, MK and YL. All authors reviewed and approved the final version of the manuscript.

Financial support

We would like to thank the Office of the Vice President of Research, University of South Carolina for the funds under COVID-19 research grants. Yuan Lin would like to thank the support from the Chinese Scholarship Council (No. 201904910172).

Acknowledgement

None.

Conflicts of interest statement

Qian Wang is an Editorial Board member of *Biomaterials Translational*.

1. Hall, C. B.; Douglas, R. G. Jr.; Geiman, J. M. Possible transmission by fomites of respiratory syncytial virus. *J Infect Dis.* **1980**, *141*, 98-102.
2. Chan, K. H.; Peiris, J. S.; Lam, S. Y.; Poon, L. L.; Yuen, K. Y.; Seto, W. H. The effects of temperature and relative humidity on the viability of the SARS coronavirus. *Adv Virol.* **2011**, *2011*, 734690.
3. van Doremalen, N.; Bushmaker, T.; Morris, D. H.; Holbrook, M. G.; Gamble, A.; Williamson, B. N.; Tamin, A.; Harcourt, J. L.; Thornburg, N. J.; Gerber, S. I.; Lloyd-Smith, J. O.; de Wit, E.; Munster, V. J. Aerosol and surface stability of SARS-CoV-2 as compared with SARS-CoV-1. *N Engl J Med.* **2020**, *382*, 1564-1567.
4. Chin, A. W. H.; Chu, J. T. S.; Perera, M. R. A.; Hui, K. P. Y.; Yen, H. L.; Chan, M. C. W.; Peiris, M.; Poon, L. L. M. Stability of SARS-CoV-2 in different environmental conditions. *Lancet Microbe.* **2020**, *1*, e10.

5. Azuma, K.; Yanagi, U.; Kagi, N.; Kim, H.; Ogata, M.; Hayashi, M. Environmental factors involved in SARS-CoV-2 transmission: effect and role of indoor environmental quality in the strategy for COVID-19 infection control. *Environ Health Prev Med.* **2020**, *25*, 66.
6. Biryukov, J.; Boydston, J. A.; Dunning, R. A.; Yeager, J. J.; Wood, S.; Reese, A. L.; Ferris, A.; Miller, D.; Weaver, W.; Zeitouni, N. E.; Phillips, A.; Freeburger, D.; Hooper, I.; Ratnesar-Shumate, S.; Yolitz, J.; Krause, M.; Williams, G.; Dawson, D. G.; Herzog, A.; Dabisch, P.; Wahl, V.; Hevey, M. C.; Altamura, L. A. Increasing temperature and relative humidity accelerates inactivation of SARS-CoV-2 on surfaces. *mSphere.* **2020**, *5*:e00441-20.
7. Chen, Y. C.; Huang, L. M.; Chan, C. C.; Su, C. P.; Chang, S. C.; Chang, Y. Y.; Chen, M. L.; Hung, C. C.; Chen, W. J.; Lin, F. Y.; Lee, Y. T. SARS in hospital emergency room. *Emerg Infect Dis.* **2004**, *10*, 782-788.
8. Stilianakis, N. I.; Drossinos, Y. Dynamics of infectious disease transmission by inhalable respiratory droplets. *J R Soc Interface.* **2010**, *7*, 1355-1366.
9. Wei, J.; Li, Y. Airborne spread of infectious agents in the indoor environment. *Am J Infect Control.* **2016**, *44*, S102-108.
10. Liu, L.; Li, Y.; Nielsen, P. V.; Wei, J.; Jensen, R. L. Short-range airborne transmission of expiratory droplets between two people. *Indoor Air.* **2017**, *27*, 452-462.
11. National Center for Immunization and Respiratory Diseases (NCIRD), Division of Viral Diseases. Public health guidance for potential COVID-19 exposure associated with travel. https://www.cdc.gov/coronavirus/2019-ncov/php/risk-assessment.html. Accessed by March 30, 2020.
12. Omer, S. B.; Malani, P.; Del Rio, C. The COVID-19 pandemic in the US: a clinical update. *JAMA.* **2020**, *323*, 1767-1768.
13. Read, R. A choir decided to go ahead with rehearsal. Now dozens of members have COVID-19 and two are dead. Los Angeles Times. https://www.latimes.com/world-nation/story/2020-03-29/coronavirus-choir-outbreak. Accessed by March 1, 2021.
14. Correia, G.; Rodrigues, L.; Gameiro da Silva, M.; Gonçalves, T. Airborne route and bad use of ventilation systems as non-negligible factors in SARS-CoV-2 transmission. *Med Hypotheses.* **2020**, *141*, 109781.
15. Morrison, G.; Lakey, P. S. J.; Abbatt, J.; Shiraiwa, M. Indoor boundary layer chemistry modeling. *Indoor Air.* **2019**, *29*, 956-967.
16. K. Lai, A. C.; Nazaroff, W. W. Modeling indoor particle deposition from turbulent flow onto smooth surfaces. *J Aerosol Sci.* **2000**, *31*, 463-476.
17. Ziskind, G.; Fichman, M.; Gutfinger, C. Effects of shear on particle motion near a surface—application to resuspension. *J Aerosol Sci.* **1998**, *29*, 323-338.
18. Göransson, A.; Trägårdh, C. Mechanisms responsible for sub-micron particle deposition in a laminar wall-jet. *Colloids Surf Physicochem Eng Aspects.* **2002**, *211*, 133-144.
19. Sjollema, J.; Busscher, H. J.; Weerkamp, A. H. Deposition of oral streptococci and polystyrene latices onto glass in a parallel plate flow cell. *Biofouling.* **1988**, *1*, 101-112.
20. Busscher, H. J.; van der Mei, H. C. Microbial adhesion in flow displacement systems. *Clin Microbiol Rev.* **2006**, *19*, 127-141.
21. Mitik-Dineva, N.; Wang, J.; Truong, V. K.; Stoddart, P.; Malherbe, F.; Crawford, R. J.; Ivanova, E. P. Escherichia coli, Pseudomonas aeruginosa, and Staphylococcus aureus attachment patterns on glass surfaces with nanoscale roughness. *Curr Microbiol.* **2009**, *58*, 268-273.
22. Kesavan, J. S.; Humphreys, P. D.; Bottiger, J. R.; Valdes, E. R.; Rastogi, V. K.; Knox, C. K. Deposition method, relative humidity, and surface property effects of bacterial spore reaerosolization via pulsed air jet. *Aerosol Sci Technol.* **2017**, *51*, 1027-1034.
23. Hruby, D. E.; Guarino, L. A.; Kates, J. R. Vaccinia virus replication. I. Requirement for the host-cell nucleus. *J Virol.* **1979**, *29*, 705-715.
24. Mendoza, E. J.; Manguiat, K.; Wood, H.; Drebot, M. Two detailed plaque assay protocols for the quantification of infectious SARS-CoV-2. *Curr Protoc Microbiol.* **2020**, *57*, ecpmc105.
25. Lee, J.; Jang, J.; Akin, D.; Savran, C. A.; Bashir, R. Real-time detection of airborne viruses on a mass-sensitive device. *Appl Phys Lett.* **2008**, *93*, 13901.
26. Peduru Hewa, T. M.; Tannock, G. A.; Mainwaring, D. E.; Harrison, S.; Fecondo, J. V. The detection of influenza A and B viruses in clinical specimens using a quartz crystal microbalance. *J Virol Methods.* **2009**, *162*, 14-21.
27. Jaiswal, A.; Smoukov, S.; Poggi, M.; Grzybowski, B. Quartz crystal microbalance with dissipation monitoring (QCM-D): real-time characterization of nano-scale interactions at surfaces. In Proceedings of the 2008 NSTI Nanotechnology Conference and Trade, Bosten, 2008.
28. Hook, F.; Rodahl, M.; Brzezinski, P.; Kasemo, B. Energy dissipation kinetics for protein and antibody-antigen adsorption under shear oscillation on a quartz crystal microbalance. *Langmuir.* **1998**, *14*, 729-734.
29. Jordan, J. L.; Fernandez, E. J. QCM-D sensitivity to protein adsorption reversibility. *Biotechnol Bioeng.* **2008**, *101*, 837-842.
30. Dixon, M. C. Quartz crystal microbalance with dissipation monitoring: enabling real-time characterization of biological materials and their interactions. *J Biomol Tech.* **2008**, *19*, 151-158.
31. Dunér, G.; Thormann, E.; Dėdinaitė, A. Quartz crystal microbalance with dissipation (QCM-D) studies of the viscoelastic response from a continuously growing grafted polyelectrolyte layer. *J Colloid Interface Sci.* **2013**, *408*, 229-234.
32. Doliška, A.; Ribitsch, V.; Stana Kleinschek, K.; Strnad, S. Viscoelastic properties of fibrinogen adsorbed onto poly(ethylene terephthalate) surfaces by QCM-D. *Carbohydr Polym.* **2013**, *93*, 246-255.
33. Roberts, K. L.; Smith, G. L. Vaccinia virus morphogenesis and dissemination. *Trends Microbiol.* **2008**, *16*, 472-479.
34. Kaufman, H. L.; Kohlhapp, F. J.; Zloza, A. Oncolytic viruses: a new class of immunotherapy drugs. *Nat Rev Drug Discov.* **2015**, *14*, 642-662.
35. Guo, Z. S.; Lu, B.; Guo, Z.; Giehl, E.; Feist, M.; Dai, E.; Liu, W.; Storkus, W. J.; He, Y.; Liu, Z.; Bartlett, D. L. Vaccinia virus-mediated cancer immunotherapy: cancer vaccines and oncolytics. *J Immunother Cancer.* **2019**, *7*, 6.
36. Dubochet, J.; Adrian, M.; Richter, K.; Garces, J.; Wittek, R. Structure of intracellular mature vaccinia virus observed by cryoelectron microscopy. *J Virol.* **1994**, *68*, 1935-1941.
37. Condit, R. C.; Moussatche, N.; Traktman, P. In a nutshell: structure and assembly of the vaccinia virion. *Adv Virus Res.* **2006**, *66*, 31-124.
38. Michen, B.; Graule, T. Isoelectric points of viruses. *J Appl Microbiol.* ***2010***, *109*, 388-397.
39. Roberts, P. Efficient removal of viruses by a novel polyvinylidene fluoride membrane filter. *J Virol Methods.* **1997**, *65*, 27-31.
40. Cyrklaff, M.; Risco, C.; Fernández, J. J.; Jiménez, M. V.; Estéban, M.; Baumeister, W.; Carrascosa, J. L. Cryo-electron tomography of vaccinia virus. *Proc Natl Acad Sci U S A.* **2005**, *102*, 2772-2777.

41. Martin, R. M.; Burke, K.; Verma, D.; Xie, H.; Langer, J.; Schlaberg, R.; Swaminathan, S.; Hanson, K. E. Contact transmission of vaccinia to an infant diagnosed by viral culture and metagenomic sequencing. *Open Forum Infect Dis.* **2020**, *7*, ofaa111.
42. Takahashi, K.; Fukuzaki, S. Cleanability of titanium and stainless steel particles in relation to surface charge aspects. *Biocontrol Sci.* **2008**, *13*, 9-16.
43. Thatcher, T. L.; Fairchild, W. A.; Nazaroff, W. W. Particle deposition from natural convection enclosure flow onto smooth surfaces. *Aerosol Sci Technol.* **1996**, *25*, 359-374.
44. Thatcher, T. L.; Layton, D. W. Deposition, resuspension, and penetration of particles within a residence. *Atmos Environ.* **1995**, *29*, 1487-1497.
45. Lai, A. C. Particle deposition indoors: a review. *Indoor Air.* **2002**, *12*, 211-214.
46. Zhao, B.; Wu, J. Particle deposition in indoor environments: analysis of influencing factors. *J Hazard Mater.* **2007**, *147*, 439-448.
47. Hoque, S.; Omar, F. B. Coupling computational fluid dynamics simulations and statistical moments for designing healthy indoor spaces. *Int J Environ Res Public Health.* **2019**, *16*, 800.
48. El Hamdani, S.; Limam, K.; Abadie, M. O.; Bendou, A. Deposition of fine particles on building internal surfaces. *Atmos Environ.* **2008**, *42*, 8893-8901.
49. Wang, Y.; Li, A.; Fan, X.; Shang, L.; Lu, S. Effects of surface properties of vertical textiles indoors on particle deposition: a small-scale chamber study. *Aerosol Air Qual Res.* **2019**, *19*, 885-895.
50. Nazaroff, W.; Gadgil, A.; Weschler, C. Critique of the use of deposition velocity in modeling indoor air quality. In *Modeling of indoor air quality and exposure*, Nagda, N., ed. ASTM International: West Conshohocken, PA, **1993**; pp 81-104.
51. Abadie, M.; Limam, K.; Allard, F. Indoor particle pollution: effect of wall textures on particle deposition. *Build Environ.* **2001**, *36*, 821-827.
52. Lai, A. C. K.; Nazaroff, W. W. Supermicron particle deposition from turbulent chamber flow onto smooth and rough vertical surfaces. *Atmos Environ.* **2005**, *39*, 4893-4900.
53. Wong, L. T.; Chan, W. Y.; Mui, K. W.; Lai, A. C. K. An Experimental and Numerical Study on Deposition of Bioaerosols in a Scaled Chamber. *Aerosol Sci Technol.* **2010**, *44*, 117-128.
54. Whyte, W.; Eaton, T. Deposition velocities of airborne microbe-carrying particles. *Eur J Parenter Pharm Sci.* **2016**, *21*, 45-49.
55. Seong, D.; Hoque, S. Does the presence of certain bacterial family in the microbiome indicate specific indoor environment characteristics? A factorial design approach for identifying bio-fingerprints. *Indoor Built Environ.* **2019**, *29*, 117-131.
56. Ranade, M. B. Adhesion and removal of fine particles on surfaces. *Aerosol Sci Technol.* **1987**, *7*, 161-176.
57. Corn, M. The adhesion of solid particles to solid surfaces. I. A review. *J Air Pollut Control Assoc.* **1961**, *11*, 523-528.
58. Corn, M. The adhesion of solid particles to solid surfaces. II. *J Air Pollut Control Assoc.* **1961**, *11*, 566-575.
59. Visser, J. Particle adhesion and removal: a review. *Particulate Sci Technol.* **1995**, *13*, 169-196.
60. Tan, C. L. C.; Gao, S.; Wee, B. S.; Asa-Awuku, A.; Thio, B. J. R. Adhesion of dust particles to common indoor surfaces in an air-conditioned environment. *Aerosol Sci Technol.* **2014**, *48*, 541-551.
61. Christenson, H. K. Adhesion and surface energy of mica in air and water. *J Phys Chem.* **1993**, *97*, 12034-12041.
62. Goldasteh, I.; Tian, Y.; Ahmadi, G.; R. Ferro, A. Human induced flow field and resultant particle resuspension and transport during gait cycle. *Build Environ.* **2014**, *77*, 101-109.
63. Mullins, M. E.; Michaels, L. P.; Menon, V.; Locke, B.; Ranade, M. B. Effect of geometry on particle adhesion. *Aerosol Sci Technol.* **1992**, *17*, 105-118.
64. Audry, M. C.; Ramos, S.; Charlaix, E. Adhesion between highly rough alumina surfaces: an atomic force microscope study. *J Colloid Interface Sci.* **2009**, *331*, 371-378.
65. Derjaguin, B. V.; Muller, V. M.; Toporov, Y. P. Effect of contact deformations on the adhesion of particles. *J Colloid Interface Sci.* **1975**, *53*, 314-326.
66. Nasr, B.; Ahmadi, G.; Ferro, A. R.; Dhaniyala, S. A model for particle removal from surfaces with large-scale roughness in turbulent flows. *Aerosol Sci Technol.* **2020**, *54*, 291-303.
67. Kim, Y.; Wellum, G.; Mello, K.; Strawhecker, K. E.; Thoms, R.; Giaya, A.; Wyslouzil, B. E. Effects of relative humidity and particle and surface properties on particle resuspension rates. *Aerosol Sci Technol.* **2016**, *50*, 339-352.
68. Jones, R.; Pollock, H. M.; Cleaver, J. A. S.; Hodges, C. S. Adhesion forces between glass and silicon surfaces in air studied by afm: effects of relative humidity, particle size, roughness, and surface treatment. *Langmuir.* **2002**, *18*, 8045-8055.
69. Katainen, J.; Paajanen, M.; Ahtola, E.; Pore, V.; Lahtinen, J. Adhesion as an interplay between particle size and surface roughness. *J Colloid Interface Sci.* **2006**, *304*, 524-529.
70. Bohinc, K.; Dražić, G.; Abram, A.; Jevšnik, M.; Jeršek, B.; Nipič, D.; Kurinčič, M.; Raspor, P. Metal surface characteristics dictate bacterial adhesion capacity. *Int J Adhes Adhes.* **2016**, *68*, 39-46.
71. An, Y. H.; Friedman, R. J. Concise review of mechanisms of bacterial adhesion to biomaterial surfaces. *J Biomed Mater Res.* **1998**, *43*, 338-348.
72. Ji, Y. W.; Cho, Y. J.; Lee, C. H.; Hong, S. H.; Chung, D. Y.; Kim, E. K.; Lee, H. K. Comparison of surface roughness and bacterial adhesion between cosmetic contact lenses and conventional contact lenses. *Eye Contact Lens.* **2015**, *41*, 25-33.
73. Berne, C.; Ellison, C. K.; Ducret, A.; Brun, Y. V. Bacterial adhesion at the single-cell level. *Nat Rev Microbiol.* **2018**, *16*, 616-627.
74. Bower, C. K.; McGuire, J.; Daeschel, M. A. The adhesion and detachment of bacteria and spores on food-contact surfaces. *Trends Food Sci Technol.* **1996**, *7*, 152-157.
75. Logan, B. E.; Regan, J. M. Microbial fuel cells--challenges and applications. *Environ Sci Technol.* **2006**, *40*, 5172-5180.
76. Jasevičius, R.; Baronas, R.; Kačianauskas, R.; Šimkus, R. Numerical modeling of bacterium-surface interaction by applying DEM. *Procedia Eng.* **2015**, *102*, 1408-1414.
77. Katsikogianni, M.; Missirlis, Y. F. Concise review of mechanisms of bacterial adhesion to biomaterials and of techniques used in estimating bacteria-material interactions. *Eur Cell Mater.* **2004**, *8*, 37-57.
78. Zhang, X.; Zhang, Q.; Yan, T.; Jiang, Z.; Zhang, X.; Zuo, Y. Y. Quantitatively predicting bacterial adhesion using surface free energy determined with a spectrophotometric method. *Environ Sci Technol.* **2015**, *49*, 6164-6171.
79. Bayoudh, S.; Othmane, A.; Mora, L.; Ben Ouada, H. Assessing bacterial adhesion using DLVO and XDLVO theories and the jet impingement technique. *Colloids Surf B Biointerfaces.* **2009**, *73*, 1-9.
80. van Oss, C. J. Hydrophobicity of biosurfaces — Origin, quantitative determination and interaction energies. *Colloids Surf B Biointerfaces.*

1995, *5*, 91-110.
81. Chrysikopoulos, C. V.; Syngouna, V. I. Attachment of bacteriophages MS2 and ΦX174 onto kaolinite and montmorillonite: extended-DLVO interactions. *Colloids Surf B Biointerfaces.* **2012**, *92*, 74-83.
82. Wang, X.; Şengür-Taşdemir, R.; Koyuncu, İ.; Tarabara, V. V. Lip balm drying promotes virus attachment: Characterization of lip balm coatings and XDLVO modeling. *J Colloid Interface Sci.* **2021**, *581*, 884-894.
83. Dang, H. T. T.; Tarabara, V. V. Virus deposition onto polyelectrolyte-coated surfaces: A study with bacteriophage MS2. *J Colloid Interface Sci.* **2019**, *540*, 155-166.
84. Joonaki, E.; Hassanpouryouzband, A.; Heldt, C. L.; Areo, O. Surface chemistry can unlock drivers of surface stability of SARS-CoV-2 in a variety of environmental conditions. *Chem.* **2020**, *6*, 2135-2146.
85. Katoh, I.; Tanabe, F.; Kasai, H.; Moriishi, K.; Shimasaki, N.; Shinohara, K.; Uchida, Y.; Koshiba, T.; Arakawa, S.; Morimoto, M. Potential risk of virus carryover by fabrics of personal protective gowns. *Front Public Health.* **2019**, *7*, 121.
86. Smither, S. J.; Eastaugh, L. S.; Findlay, J. S.; Lever, M. S. Experimental aerosol survival of SARS-CoV-2 in artificial saliva and tissue culture media at medium and high humidity. *Emerg Microbes Infect.* **2020**, *9*, 1415-1417.
87. Duan, S. M.; Zhao, X. S.; Wen, R. F.; Huang, J. J.; Pi, G. H.; Zhang, S. X.; Han, J.; Bi, S. L.; Ruan, L.; Dong, X. P. Stability of SARS coronavirus in human specimens and environment and its sensitivity to heating and UV irradiation. *Biomed Environ Sci.* **2003**, *16*, 246-255.
88. Knoll, J.; Dammert, W. R.; Nirschl, H. Integration of a microscope into a centrifuge for adhesion force measurement of particles. *Powder Technol.* **2017**, *305*, 147-155.
89. Kulvanich, P.; Stewart, P. J. Fundamental considerations in the measurement of adhesional forces between particles using the centrifuge method. *Int J Pharm.* **1987**, *35*, 111-120.
90. Huang, R.; Yi, P.; Tang, Y. Probing the interactions of organic molecules, nanomaterials, and microbes with solid surfaces using quartz crystal microbalances: methodology, advantages, and limitations. *Environ Sci Process Impacts.* **2017**, *19*, 793-811.
91. Page, K.; Wilson, M.; Mordan, N. J.; Chrzanowski, W.; Knowles, J.; Parkin, I. P. Study of the adhesion of Staphylococcus aureus to coated glass substrates. *J Mater Sci.* **2011**, *46*, 6355-6363.
92. Yakub, I.; Soboyejo, W. O. Adhesion of E. coli to silver- or copper-coated porous clay ceramic surfaces. *J Appl Phys.* **2012**, *111*, 124324.
93. Liu, Z.; Niu, H.; Rong, R.; Cao, G.; He, B. J.; Deng, Q. An experiment and numerical study of resuspension of fungal spore particles from HVAC ducts. *Sci Total Environ.* **2020**, *708*, 134742.
94. Feigley, C.; Khan, J.; Salzberg, D.; Hussey, J.; Attaway, H.; Steed, L.; Schmidt, M.; Michels, H. Experimental tests of copper components in ventilation systems for microbial control. *HVAC&R Res.* **2013**, *19*, 53-62.
95. Tamburini, E.; Donegà, V.; Marchetti, M. G.; Pedrini, P.; Monticelli, C.; Balbo, A. Study on microbial deposition and contamination onto six surfaces commonly used in chemical and microbiological laboratories. *Int J Environ Res Public Health.* **2015**, *12*, 8295-8311.
96. Villapún, V. M.; Dover, L. G.; Cross, A.; González, S. Antibacterial metallic touch surfaces. *Materials (Basel).* **2016**, *9*, 736.
97. Hoang, C. P.; Kinney, K. A.; Corsi, R. L.; Szaniszlo, P. J. Resistance of green building materials to fungal growth. *Int Biodeterior Biodegrad.* **2010**, *64*, 104-113.
98. Straub, H.; Bigger, C. M.; Valentin, J.; Abt, D.; Qin, X. H.; Eberl, L.; Maniura-Weber, K.; Ren, Q. Bacterial adhesion on soft materials: passive physicochemical interactions or active bacterial mechanosensing? *Adv Healthc Mater.* **2019**, *8*, e1801323.
99. Loosmore, G. A. Evaluation and development of models for resuspension of aerosols at short times after deposition. *Atmos Environ.* **2003**, *37*, 639-647.
100. Ibrahim, A. H.; Brach, R. M.; Dunn, P. F. Microparticle detachment from surfaces exposed to turbulent air flow: microparticle motion after detachment. *J Aerosol Sci.* **2004**, *35*, 1189-1204.
101. Punrath, J. S.; Heldman, D. R. Mechanisms of small particle re-entrainment from flat surfaces. *J Aerosol Sci.* **1972**, *3*, 429-440.
102. Braaten, D. A.; Paw U, K. T.; Shaw, R. H. Particle resuspension in a turbulent boundary layer-observed and modeled. *J Aerosol Sci.* **1990**, *21*, 613-628.
103. G. Ziskind. Particle resuspension from surfaces: revisited and re-evaluated. *Rev Chem Eng.* **2006**, *22*, 1-123.
104. Ziskind, G.; Fichman, M.; Gutfinger, C. Resuspension of particulates from surfaces to turbulent flows—Review and analysis. *J Aerosol Sci.* **1995**, *26*, 613-644.
105. Kim, Y.; Gidwani, A.; Wyslouzil, B. E.; Sohn, C. W. Source term models for fine particle resuspension from indoor surfaces. *Build Environ.* **2010**, *45*, 1854-1865.
106. Cheng, Z.; Yu, X.; Hsu, T. J.; Balachandar, S. A numerical investigation of fine sediment resuspension in the wave boundary layer—Uncertainties in particle inertia and hindered settling. *Comput Geosci.* **2015**, *83*, 176-192.
107. Ji, S.; Ouahsine, A.; Smaoui, H.; Sergent, P. 3D numerical modeling of sediment resuspension induced by the compounding effects of ship-generated waves and the ship propeller. *J Eng Mech.* **2014**, *140*, 04014034.
108. Wang, R. Q.; Law, A. W. K.; Adams, E. E. Large-eddy simulation (LES) of settling particle cloud dynamics. *Int J Multiphase Flow.* **2014**, *67*, 65-75.
109. Saffman, P. G. The lift on a small sphere in a slow shear flow. *J Fluid Mech.* **1965**, *22*, 385-400.
110. Mollinger, A. M.; Nieuwstadt, F. T. M. Measurement of the lift force on a particle fixed to the wall in the viscous sublayer of a fully developed turbulent boundary layer. *J Fluid Mech.* **1996**, *316*, 285-306.
111. Leighton, D.; Acrivos, A. The lift on a small sphere touching a plane in the presence of a simple shear flow. *Z Angew Math Phys.* **1985**, *36*, 174-178.
112. Shi, L.; Bayless, D. J. Comparison of boundary conditions for predicting the collection efficiency of cyclones. *Powder Technol.* **2007**, *173*, 29-37.
113. Benito, J. G.; Aracena, K. A. V.; Uñac, R. O.; Vidales, A. M.; Ippolito, I. Monte Carlo modelling of particle resuspension on a flat surface. *J Aerosol Sci.* **2015**, *79*, 126-139.
114. Henry, C.; Minier, J. P. A stochastic approach for the simulation of particle resuspension from rough substrates: Model and numerical implementation. *J Aerosol Sci.* **2014**, *77*, 168-192.
115. Ferro, A. R.; Kopperud, R. J.; Hildemann, L. M. Source strengths for indoor human activities that resuspend particulate matter. *Environ Sci Technol.* **2004**, *38*, 1759-1764.
116. Krauter, P.; Biermann, A. Reaerosolization of fluidized spores in ventilation systems. *Appl Environ Microbiol.* **2007**, *73*, 2165-2172.

Received: January 17, 2021
Revised: March 8, 2021
Accepted: March 21, 2021
Available online: March 28, 2021